ISIJ International, Vol. 42 (2002), No. 1, pp. 80–85

Effect of Mg and Si on the Microstructure and Corrosion Behavior of Zn–Al Hot Dip Coatings on Low Carbon Steel

Junichi TANAKA, Keisuke ONO,[1)] Shigenari HAYASHI, Kenichi OHSASA and Toshio NARITA

Research Group of Interface Control Engineering, Graduate School of Engineering, Hokkaido University, Kita-ku, Sapporo 060-8628 Japan. 1) Graduate Student, Graduate School of Engineering, Hokkaido University, Kita-ku, Sapporo 060-8628 Japan.

(*Received on April 9, 2001; accepted in final form on September 9, 2001*)

Coatings formed on a low carbon steel by a two step hot dipping, primarily in a Zn bath and secondarily in a Zn–6Al bath with or without 0.5 mass% Mg and 0.1 mass% Si addition. The effects of the Mg and Si addition on the surface morphologies, microstructures, and corrosion characteristics of the coatings were investigated using a scanning electron microscope, a laser scanning microscope, and an electron probe microprobe analyzer. The coating formed in the Zn–6Al bath showed flaws as pores and cracks in the outer adhered layer, while there were few flaws in the Zn–6Al–0.5Mg–0.1Si bath coating. The Zn–6Al–0.5Mg–0.1Si coating has a lamellae structure developed well in the outer adhered layer and the initially formed α-Al was finer than that of the Zn–6Al coating. Corrosion in a 5% NaCl solution commenced from the α-Al phase at a very early stage and the Zn phase corroded preferentially. The Zn–6Al–0.5Mg–0.1Si coating corroded slowly and relatively homogeneously, while the Zn–6Al coating degraded locally due to a preferential corrosion along flaws. The Zn–6Al–0.5Mg–0.1Si coating incorporates Mg and Si in the outer adhered layer and Si in the inner alloy layer, making the Zn–6Al–0.5Mg–0.1Si coating more anti-corrosive.

KEY WORDS: low carbon steel; two step hot dipping; Zn–Al coating; Zn–Al–Mg–Si coating; corrosion behavior; solidification structure.

1. Introduction

Structural steels with a Zn–Al coating have been used in aggressive environments such as shore side areas, because of their good corrosion resistance.[1–4)] Coatings of more than 50 μm thickness are usually made by dipping steels in a Zn–Al bath containing more than 6 mass% Al and this is then heat treated to form a duplex structure of inner alloy layer and outer adhered layer. Although Zn–Al coated steel, like Galfan has showed good corrosion resistance, it suffers from poor performance under long durations in aggressive environments. One weak point is flaws such as holes and cracks formed in the outer adhered layer during solidification, and another is preferential attacks along the periphery of the α-Al phase which precipitates from baths containing more than 6 mass% Al. Many papers[5,6)] have dealt with addition of alloying elements to the alloying bath to improve the anti-corrosion properties of the coating, however these coatings are thin and directed to use with automobiles. For relatively thick coating of structural steels, there is little information on the effect of foreign additional elements, except the papers by Komatsu *et al*.[7–9)] They added Mg to the Zn–Al alloy bath and investigated the corrosion behavior of the Zn–6Al–Mg coating, showing a beneficial effect of Mg in prevention of corrosion. However, details of the Mg effect on the surface morphology and coating structure are still not entirely clear.

The two step hot dipping method, which consists of dipping in first a Zn bath and then in a Zn–6Al bath has been investigated and it was demonstrated that the two step hot dipping has advantages such as good adhesion of the coating,[10,11)] and the feasibility of controlling thickness and microstructure. Morphology and microstructure of the coating has been controlled by bath temperatures and dipping times.

The purpose of this investigation is to elucidate the effect of Mg and Si addition to the secondary Zn–Al bath on the surface morphology and the microstructure of the coating formed by the two step hot dipping. The corrosion behavior of an inner alloy layer and an outer adhered layer of the Zn–Al coatings with and without Mg and Si is examined and discussed based on microstructural features.

2. Experimental Procedures

The experiments used the low carbon steel with a nominal composition (mass%) of 0.2Mn, 0.08C, 0.04Si, 0.02C, 0.01P, 0.01S, and Fe remaining. A $30\times50\times3$ mm^3 sample was degreased in a 8% NaOH aqueous solution at 353 K for 3.6 ks, and then the surface oxide scale was removed in a 15% HCl aqueous solution at 333 K for 60 s. This specimen was immersed in a 35%$ZnCl_2+NH_4Cl$ (1 : 3) solution at 333 K for 15 s, and then dried in air. After drying, the specimen was dipped first in a Zn (99.99%purity) bath at 743 K for 60 s and then immediately after in a Zn–Al or Zn–Al–Mg–Si bath at 743 K for 60 s. The secondary Zn–Al

bath contains 6 mass% Al and Zn remaining, and the Zn–Al–Mg–Si bath was prepared by adding 0.5 mass% Mg and 0.1 mass% Si to the Zn–6 mass%Al melt. The Zn–6 mass%Al bath is referred as the Z6A bath and the Zn–6 mass%Al–0.5 mass%Mg–0.1 mass%Si bath as the Z6AMS bath in this paper, and the coatings formed in the Z6A and Z6AMS baths are Z6A and Z6AMS coatings, respectively. After dipping in the secondary baths, the specimens were cooled for 15 s in air and then quenched in water.

Surface morphology and cross-sectional microstructure of the coatings were observed using optical-, scanning electron- and laser-scanning microscopes (OM, SEM, LSM). The SEM was utilized to observe surface flaws and LSM to measure undulation in the coated surface. An electron-probe micro-analyzer (EPMA) was used to measure the concentration distributions of each element. Polished cross-sections were etched slightly in a 3% nitric acid-ethanol solution to clearly show the microstructure.

Corrosion tests were conducted in a 5% NaCl aqueous solution at room temperature. Immersion times varied from 60 s to 18 ks. After corrosion the specimens were washed in water and dried, and then examined using SEM, EPMA and LSM, as described above.

3. Results and Discussion

Figure 1 shows the surface morphology of the coatings formed by the two step hot dipping with the secondary baths of Z6A (a) and Z6AMS (b). The coating from the Z6A bath contains flaws like pores and cracks on the surface, which may have formed due to shrinkage of the melts during the solidification and subsequent heat-treatment processes. The surface of the coating formed in the Z6AMS bath showed very fine grains and few flaws.

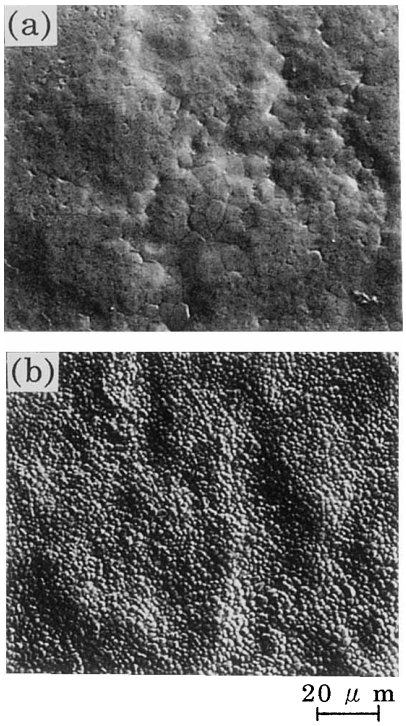

Fig. 1. Surface morphologies of the coatings formed on a low carbon steel by the two-step hot dipping. The secondary baths are (a) Zn–6Al alloy and (b) Zn–6Al–0.5Mg–0.1Si alloy.

Surface undulation was measured using LSM over areas of about 3 mm^2. Typical scanning patterns are shown in **Fig. 2**, and there are hollows in the pattern, which correspond to the holes and cracks. **Figure 3** shows the number density of flaws as a function of hollow depth. In Fig. 3 a number of flaws were counted over a central area of 1 cm^2, except a small surface undulation with several micron meters. As demonstrated in Fig. 3, the maximum depth was close to 60 μm with the Z6A coating, and the flaws occasionally reached the steel substrate. With the Z6AMS coating both the number density and maximum hollow depth was significantly smaller. The maximum depth is 30 μm, which is about half of that in the Z6A coating. The most common flaws were 30 μm deep with the Z6A coating and 10 μm with the Z6AMS coating. These vertical depths of 30 and 10 μm are close to the thickness of the outer, adhered layer of each coating.

Figure 4 shows cross sectional microstructures of the Z6A coating (a) and the Z6AMS coating (b) after the two

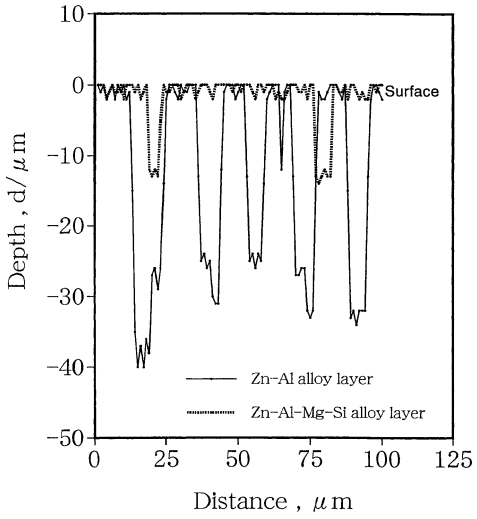

Fig. 2. Surface contour profiles measured using a laser scanning microscope for the Zn–6Al coating (a) and the Zn–6Al–0.5Mg–0.1Si coating (b) in Fig. 1.

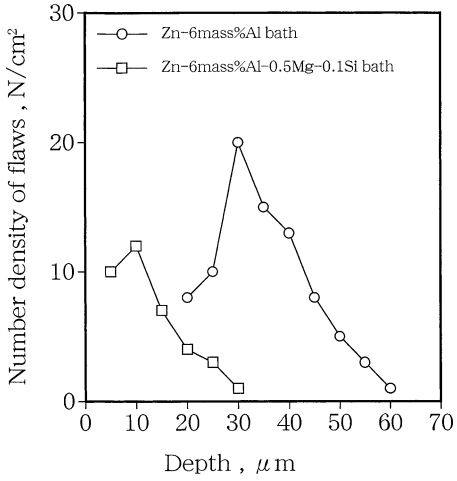

Fig. 3. Changes in number density of flaws as a function of depth of the flaws in the Zn–6Al and Zn–6Al–0.5Mg–0.1Si coated surfaces.

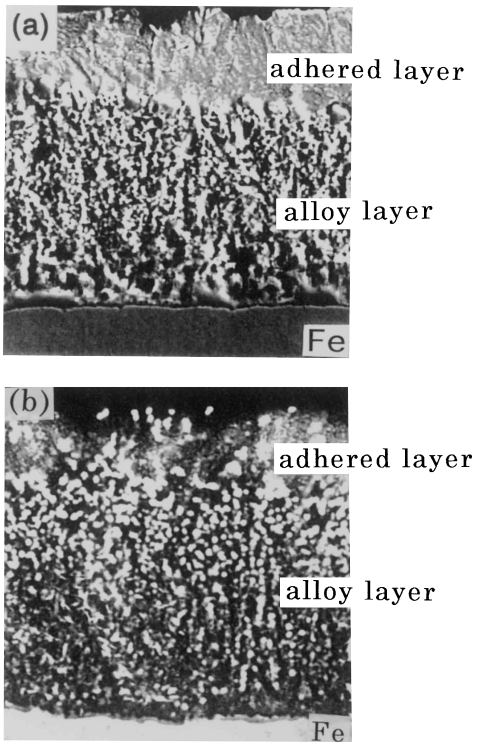

Fig. 4. Cross sectional microstructures of (a) the Zn–6Al coated and (b) the Zn–6Al–0.5Mg–0.1Si coated films.

step hot dipping. The coating layers consisted of a duplex structure; an outer, adhered layer and an inner, alloy layer. The inner alloy layer was identified to be mainly composed of an intermetallic phase of Fe_4Al_{13}–Zn surrounded by a Zn–Al melt, which penetrated and then solidified during cooling. It was observed that the Fe_4Al_{13}–Zn crystals distributed randomly in the Z6A coating, while the Z6AMS coating has a Fe_4Al_{13}–Zn phase with a columnar structure grown perpendicular to the steel substrate. Details of the microstructure and the formation mechanism of the duplex structure in the two step hot dipping have been reported in previous papers.[10,11]

Figures 5(a) and **5(b)** show the outer, adhered layer solidified during cooling of the remaining melt for the Z6A and Z6AMS coatings, respectively. In these pictures a dark area is a primarily α-Al and a bright area is an eutectic structure of Zn (Al) and α-Al. The primary α-Al was consisted of an α'-Al and Zn (Al) phases, which were transformed from the primary α-Al by the eutectoid reaction at 548 K during cooling to room temperature.[12] It was found that the primary α-Al in the Z6A coating in Fig. 5(a) was much coarser than that of the Z6AMS coating in Fig. 5(b).

Figure 6 shows X-ray mappings of Si and Mg in the cross-sections of the outer layer and alloy layer of the coating formed on the Z6AMS. It was found that Si and Mg existed in the alloy layer and outer layer, respectively. In particular Mg concentrated at a top surface of the outer layer, forming a Mg-rich oxide film with several micron meters. A formation of the Mg-rich oxide film was confirmed with characteristic features of surface color and morphology, different from those of the Z6A coating.

Figure 7 shows a schematic illustration of the formation of the outer, adhered layer in the coating during solidification for both the Z6A and Z6AMS coatings. It was assumed

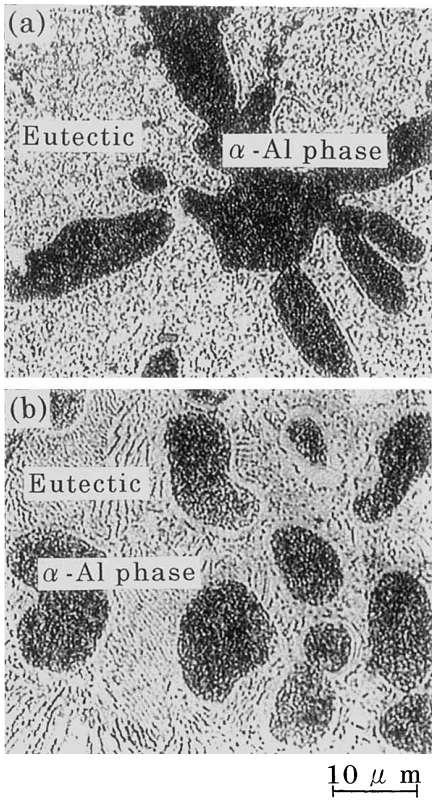

Fig. 5. Microstructures of the outer, adhered layer of (a) the Zn–6Al coated and (b) the Zn–6Al–0.5Mg–0.1Si coated films.

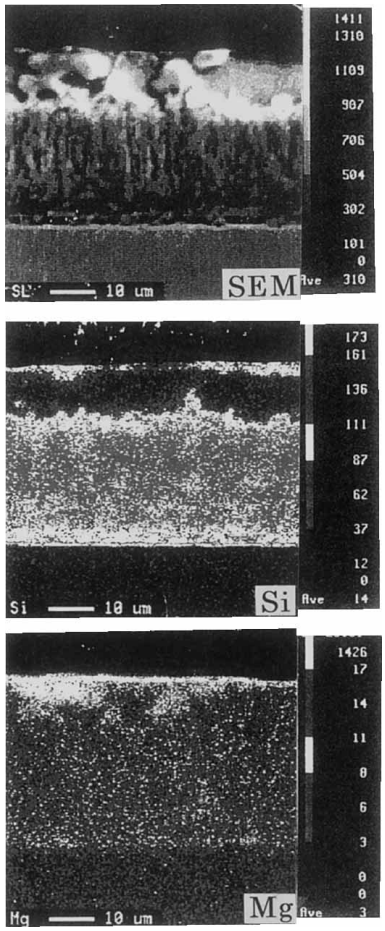

Fig. 6. X-ray images of Si and Mg in the cross-sections of the outer, adhered and alloy layers of the Zn–6Al–0.5Mg–0.1Si dipped film.

in these models that solidification commenced from the steels side and proceeded toward the melt surface, in opposite to the direction of the heat flow, forming coarse dendrite of the α-Al. In case of the Z6A coating the melt in the inter-dendrite spaces solidified in accompanying a formation of shrinkage flaws such as pores and cracks in deep, as shown in Fig. 3. While, in case of the Z6AMS coating there may be fine particles of MgO in the remaining melt and they act as nuclei for precipitation of the α-Al crystal, increasing its number density, as shown in Fig. 5. Further, the Mg-rich oxide film formed on the Z6AMS coating was relatively thick, as shown in Fig. 6, and then it might act somewhat as a thermal barrier, resulting in the coarse eutectic structure, as shown in Fig. 5. Accordingly, shrinkage flaws observed for the Z6A coating could be suppressed at final solidification of the remaining melt in the Z6AMS coating.

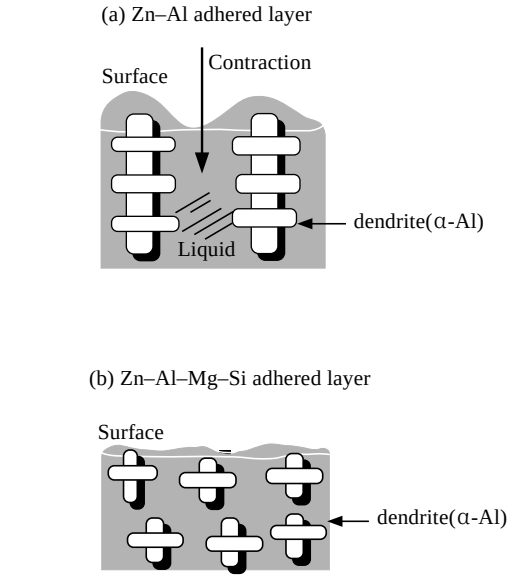

Fig. 7. Schematic representation of the solidification process in the outer, layer in (a) the Zn–6Al coated and (b) the Zn–6Al–0.5Mg–0.1Si coated films.

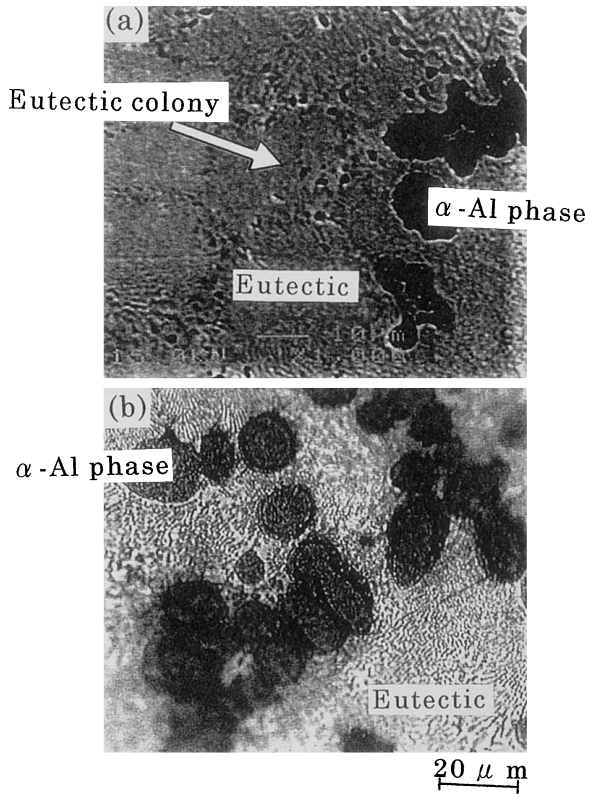

Fig. 8. Microstructures of the surface internal, adhered layer in (a) the Zn–6Al coated and (b) Zn–6Al–0.5Mg–0.1Si coated Films after corrosion in a 5% NaCl solution for 60 s at room temperature.

Figure 8 shows microstructures of the surface internal, adhered layer in the Z6A and Z6AMS coatings after corrosion in a 5% NaCl solution for 60 s at room temperature. In Fig. 8 the dark parts are the preferentially corroded areas. In the Z6A coating, corrosion was initiated at the boundaries between lamellae colonies, as shown in Fig. 8(a), and the α-Al phase tended to corrode fast. For the Z6AMS coating, as shown in Fig. 8(b), corrosion took place only in the α-Al crystals and their periphery, and the lamellae structure remained uncorroded.

Figure 9 shows changes in microstructures of the outer, adhered layer with corrosion times for both the Z6A and Z6AMS coatings. The Z6A coating suffered from severe corrosion at lamellae colony boundaries and of the Zn phase in the lamellae. The α-Al phase, which corroded fast in the initial stage in Fig. 9(a) (corrosion time 300 s), is still present. With further corrosion the α-Al phase degraded by attacking the Zn phase precipitated by the eutectoid reaction and after corrosion for 1.8 ks the original structure had disappeared, as shown in Fig. 9(a) (corrosion time 1.8 ks). Meanwhile, with the Z6AMS coating the original structure with the α-Al and lamellae structure is still present after corrosion for 1.8 ks, as shown in Fig. 9(b), although the Zn phase in and surrounding the α-Al as well as in the lamellae were corroded selectively.

Figure 10 shows changes in the microstructure of the inner, alloy layer of the Z6A and Z6AMS coatings as a function of corrosion time. With Z6A coating corrosion was observed locally, as indicated by an arrow in Fig. 10(a) (corrosion time 300 s), and it proceeded significantly for prolonged corrosion in Fig. 10(a) (corrosion time 1.8 ks). Meanwhile, corrosion of the Z6AMS coating was relatively homogeneous, although the Zn phase corroded preferentially. To verify the localized attack, the structure of the inner alloy layer was observed at high–magnification after corrosion for 1.8 ks and the micrographs are shown in **Fig. 11**. There are areas attacked severely in the Z6A coating as shown by the arrow in Fig. 11(a), while there is little localized corrosion in the Z6AMS coating.

Figure 12 shows concentration profiles of Mg and Si across the cross-section of the Z6AMS coating. Mg was found in the outer adhered layer, whereas Si concentrated in the inner alloy layer, and reached about 9 mass% at the steel/coating interface. When the Z6AMS melt penetrated into the inter-dendrite spacing the Si can alloy with the Fe–Al–Zn crystal, while it may be considered that Mg is excluded from the melt toward the outer, adhered layer. These results led to the conclusion that the Mg improves corrosion resistance of the outer, adhered layer, and that Si may improve that of the inner, alloy layer.

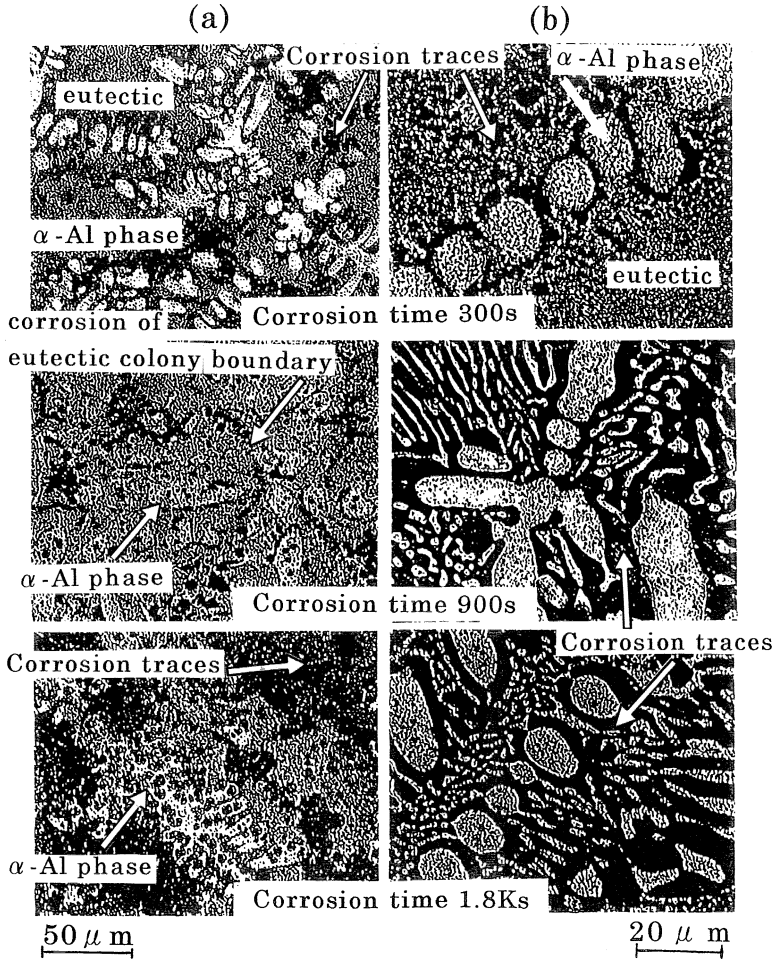

Fig. 9. Microstructures of the surface internal, adhered layer in (a) the Zn–6Al coated and (b) the Zn–6Al–0.5Mg–0.1Si coated films for different corrosion times in a 5% NaCl solution at room temperature.

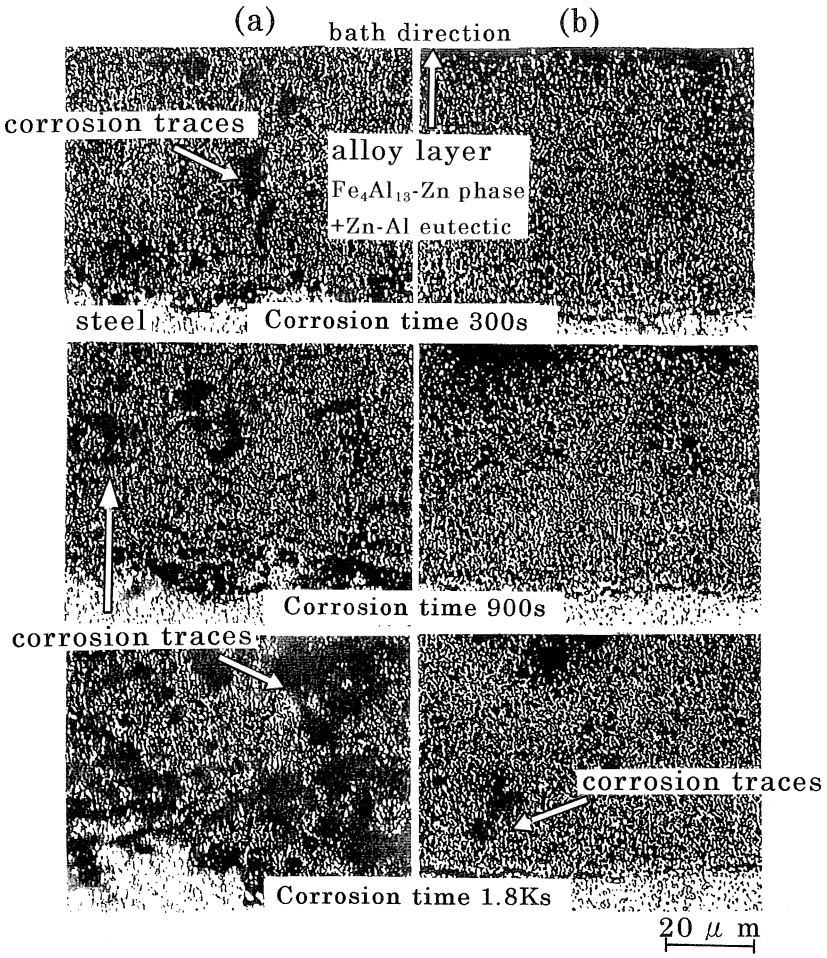

Fig. 10. Microstructures of cross-sections of the inner, alloy layer in (a) the Zn–6Al coated and the (b) Zn–6Al–0.5Mg–0.1Si coated films for different corrosion times in a 5%NaCl solution at room temperature.

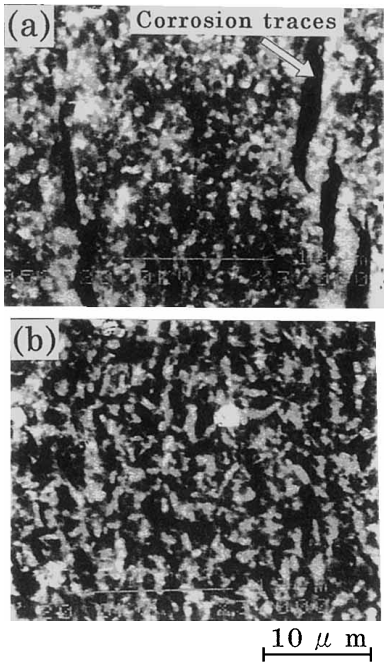

Fig. 11. Magnified SEM photographs of the cross-sections of the inner, alloy layer in (a) the Zn–6Al coat and (b) the Zn–6Al–0.5Mg–0.1Si coated film after corrosion in a 5% NaCl solution at room temperature for 1.8 ks.

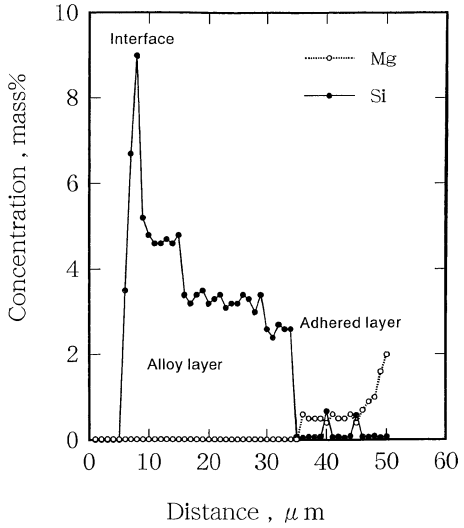

Fig. 12. Concentration profiles of Mg and Si in the Zn–6Al–0.5Mg–0.1Si coated film.

4. Conclusions

Surface morphologies and microstructures of the coatings formed on a low carbon steel by a two step hot dipping. First in a Zn bath and second in a Zn–6Al bath with and without 0.5 mass% Mg and 0.1 mass% Si addition. The corrosion behavior of the coatings was investigated in a 5% NaCl solution and is discussed based on the microstructures. The results may be summarized as follows.

(1) The Zn–6Al coating has flaws, pores and cracks, in the outer, adhered layer, while there are few flaws with the Zn–6Al–0.5Mg–0.1Si coating. Different from the Zn–6Al coating the outer adhered layer of the Zn–6Al–0.5Mg–0.1Si coating has fine α-Al crystals and a lamellae structure was well developed.

(2) The Zn–rich phase corroded in both coatings, except for the very initial stage of corrosion. The flaws in the outer adhered layer of the Zn–6Al coating corroded selectively, while corrosion of the Zn–6Al–0.5Mg–0.1Si coating was slow and relatively homogeneous.

(3) The Mg and Si were concentrated in the outer adhered layer and Si in the inner alloy layer. The Mg and Si make the Zn–6Al–0.5Mg–0.1Si coating more anti-corrosive, than the layers without these two elements.

REFERENCE

1) Y. Hirose, Y. Uchida, M. Hujita and J. Sumitani: *Tetsu-to-Hagané*, **67** (1981), S482.
2) F. E. Goodwin and S. F. Radtke: *Namari-to-Aen*, **119** (1984), 26.
3) P. Puomi, H. M. Fagerholm and J. B. Rosenholm: *Surf. Coat. Technol*., **115** (1990), 70.
4) Z. W.Chen, J. T. Gregory and R. M. Sharp: *Metall. Trans. A*, **23** (1992), 2393.
5) Y. Numakura, M. Kitajima and Y. Miyoshi: *Tetsu-to-Hagané*, **70** (1984), S1114.
6) J. Kawafuku, J. Katoh, M. Toyama, H. Nishimoto, K. Ikeda and H. Satoh: *Tetsu-to-Hagané*, **77** (1991), 995.
7) A. Komatsu, H. Izutani, T. Tsujimura A. Andoh and T. Kittaka: *Tetsu-to-Hagané*, **86** (2000), 36.
8) A. Komatsu, T. Tsujimura, H. Izutani, A. Andoh and T. Kittaka: *CAMP-ISIJ*, **12** (1999), 1346.
9) A. Komatsu, T. Tsujimura and A. Andoh: *CAMP-ISIJ*, **13** (2000), 589.
10) J. Tanaka, Y. Masuda, T. Takeichi, M. Sakaguchi and T. Narita: *Hyomengijutsu*, **48** (1997), 929.
11) J. Tanaka, R. Masumoto, K. Ohsasa and T. Narita: *Hyomengijutsu*, **48** (1997), 1012.
12) M. Ochiai and H. Ohba: *Tetsu-to-Hagané*, **75** (1989), 290.